

Towards the Causal Complete Cause of Multi-Modal Representation Learning

Jingyao Wang^{1 2 *} Siyu Zhao^{2 *} Wenwen Qiang^{1 2} Jiangmeng Li^{1 2} Fuchun Sun^{1 3} Hui Xiong⁴

Abstract

Multi-Modal Learning (MML) aims to learn effective representations across modalities for accurate predictions. Existing methods typically focus on modality consistency and specificity to learn effective representations. However, from a causal perspective, they may lead to representations that contain insufficient and unnecessary information. To address this, we propose that effective MML representations should be causally sufficient and necessary. Considering practical issues like spurious correlations and modality conflicts, we relax the exogeneity and monotonicity assumptions prevalent in prior works and explore the concepts specific to MML, i.e., Causal Complete Cause (C^3). We begin by defining C^3 , which quantifies the probability of representations being causally sufficient and necessary. We then discuss the identifiability of C^3 and introduce an instrumental variable to support identifying C^3 with non-exogeneity and non-monotonicity. Building on this, we conduct the C^3 measurement, i.e., C^3 risk. We propose a twin network to estimate it through (i) the real-world branch: utilizing the instrumental variable for sufficiency, and (ii) the hypothetical-world branch: applying gradient-based counterfactual modeling for necessity. Theoretical analyses confirm its reliability. Based on these results, we propose C^3 Regularization, a plug-and-play method that enforces the causal completeness of the learned representations by minimizing C^3 risk. Extensive experiments demonstrate its effectiveness.

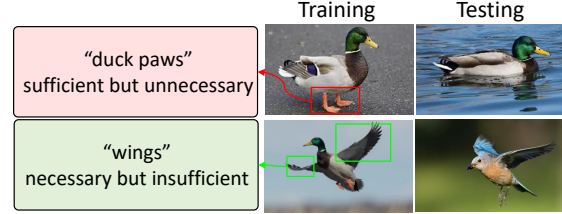


Figure 1: Example of causal sufficiency and necessity in “duck” classification task (See Section 2 for more analyses).

1. Introduction

The initial inspiration for artificial intelligence is to imitate human perceptions which are based on different modalities (Jordan & Mitchell, 2015; Mahesh, 2020), e.g., sight, sound, and touch. Each modality provides unique information with distinct properties (Baltrušaitis et al., 2018; Wang et al., 2023c). Multi-modal learning (MML) (Huang et al., 2021a; Ge et al., 2023) has emerged as a promising approach to emulate human perception. It aims to learn good representations from multiple modalities for accurate decisions.

In this context, a key question arises: what defines a “good” MML representation? Existing methods typically define good MML representations from two perspectives: modality consistency and modality specificity (Zhang et al., 2023a; Ge et al., 2023; Radford et al., 2021; Fan et al., 2024; Dong et al., 2024). The former emphasizes extracting modality-shared semantics related to primary events within the MML task. This type of methods (Liang et al., 2022; Xia et al., 2024; Abdollahzadeh et al., 2021) aims to obtain unified representations by mapping features from different modalities into a common embedding space. In contrast, the second perspective believes modality specificity captures the distinct statistical properties of each modality, reflecting different aspects of the primary events. This type of methods (Dong et al., 2024; Yang et al., 2022; Frost et al., 2015; Zhou et al., 2021) decomposes features within each modality into modality-specific and modality-shared components, learning all shared components while applying distance constraints on modality-specific features to enhance diversity.

However, from a causal perspective (Ahuja et al., 2020; Koyama & Yamaguchi, 2020), these methods may result in the learned representations being insufficient or unnecessary. Specifically, sufficiency indicates that the use of the repre-

^{*}Equal contribution ¹Institute of Software Chinese Academy of Sciences, Beijing, China ²University of the Chinese Academy of Sciences, Beijing, China ³Tsinghua University, Beijing, China ⁴Hong Kong University of Science and Technology, Hong Kong SAR, China. Correspondence to: Wenwen Qiang <qiangwenwen@iscas.ac.cn>.

representations will establish the label, while necessity indicates that the label becomes incorrect when the representations are absent (Pearl, 2009). **Figure 1** provides an example. If the MML model only focuses on causal sufficiency, it will lose important modality-specific semantics, affecting generalization; if the model only focuses on causal necessity, the decisions may be made incorrectly based on the background, affecting discriminability. Correspondingly, considering the aforementioned two types of MML methods: (i) those focused on modality consistency may cause the model to overlook important modality-specific semantics; (ii) those focused on modality specificity may incorrectly capture irrelevant information. Thus, existing MML methods (Dong et al., 2024; Lu et al., 2022) without causal constraints may fail to satisfy sufficiency and necessity, affecting model performance. The experiments in **Section 6.2** further prove this (**Figure 3** and **Table 1**): (i) the representations learned by existing methods have much lower correlation scores with sufficient and necessary causes than the proposed method with specific constraints; (ii) after constraining the learned representations, the performance of existing MML methods are significantly improved. The analyses in **Section 4** also emphasize the importance of causal sufficiency and necessity. Thus, inspired by (Pearl, 2009; Yang et al., 2024), we propose that a good MML representation must with both causal sufficiency and necessity, i.e., being causal complete.

Noticeably, in practical MML applications, constraining the causal sufficiency and necessity of learned representations remains challenging. Specifically, the related discussion in existing works (Yang et al., 2024; Pearl, 2009) are based on the exogeneity and monotonicity assumptions (**Definition D.1** and **Definition D.2** in **Appendix D.4**). Exogeneity refers to the scenario where the influence of the external intervention on the conditional distributions is negligible when the causal representation variable is exogenous relative to label variable, while monotonicity illustrates the consistent, unidirectional effect on the label variable of representation variable. However, in practice, non-trivial corner cases often arise: the inseparability of MML semantics leads to spurious correlations (**Figure 2**), and cross-modal conflicts combined with high-dimensional nonlinear interactions (Huang et al., 2021b; Wang et al., 2023d) undermine monotonicity. These challenges render the conditions of traditional causal sufficiency and necessity discussion inapplicable.

To address this, in this paper, we relax the above assumptions to explore the causal sufficiency and necessity in MML, ensuring the quality of the learned representation. Firstly, we propose the definition of causal sufficiency and necessity, i.e., causal complete causes (C^3), for MML based on (Pearl, 2009). It reflects the probability that the learned representation is causally complete by estimating the probability of label change after an intervention on the representation given two conditions of observations. One condition is for

sufficiency, and another is for necessity. Then, we analyze the identifiability of C^3 , which allows us to quantify C^3 using the observable data in practice. Unlike previous studies, we propose an instrumental variable to ensure estimating the segmented effect of C^3 without spurious correlations, thereby relaxing the assumptions of exogeneity and monotonicity. Based on this, we propose the measurement of C^3 using the twin network, i.e., C^3 risk, where a low C^3 risk means that the learned representations are causally complete with high confidence. The challenge of C^3 measurement lies in eliminating the spurious correlations in the sufficiency evaluation and modeling the counterfactual data required for the necessity evaluation. The proposed twin network addresses this through (i) the real-world branch: using the proposed instrumental variable to eliminate spurious correlations in the representation, and (ii) the hypothetical-world branch: using provable gradient-based adjustments to model the counterfactuals. Through theoretical analyses, we prove the reliability of the twin network and provide the performance guarantee of the C^3 risk. Based on these theoretical results, we propose Causal Complete Cause Regularization (C^3R), a plug-and-play method to learn causal complete representations by constraining their C^3 risks.

The main contributions are as follows: (i) We propose the definition, identifiability, and measurement of the causal complete cause (C^3) concept for MML without the assumptions of exogeneity and monotonicity. These results provide an effective way, i.e., C^3 risk, to estimate the sufficiency and necessity of the learned representation for robust and accurate MML (**Section 3**). (ii) We theoretically demonstrate the effectiveness and reliability of the proposed C^3 risk. Inspired by this, we propose C^3R , which can be applied to any MML model to learn causal complete representations with low C^3 risk ((**Sections 4 and 5**)). (iii) Finally, we conduct extensive experiments on various datasets that prove the effectiveness and robustness of C^3R (**Section 6**).

2. Problem Analysis

Problem Settings Let \mathcal{X} , \mathcal{Y} , and \mathcal{Z} represent the input space, label space, and latent space, respectively. Consider a MML task involving data $(x, y) \in \mathcal{X} \times \mathcal{Y}$, where $x \in \mathcal{X}$ denotes the sample and $y \in \mathcal{Y}$ denotes the label. All the data are sampled from the same joint distribution P_{XY} over $\mathcal{X} \times \mathcal{Y}$. The training dataset is defined as $\mathcal{D}_{tr} = \{(x_i, y_i)\}_{i=1}^N$, and the testing dataset is defined as \mathcal{D}_{te} . Here, each sample $x_i = \{x_i^{(1)}, \dots, x_i^{(K)}\}$ contains K modalities. The objective of MML is to obtain a robust model $f_\theta = \mathcal{W} \circ g$ that performs well on unseen test dataset \mathcal{D}_{te} . Here, the $g : \mathcal{X} \rightarrow \mathcal{Z}$ is the feature extractor and $\mathcal{W} : \mathcal{Z} \rightarrow \mathcal{Y}$ is the classifier. The specific implementation is illustrated in **Appendix G**, and the table of notations is shown in **Table 4**.

From the perspective of data generation (Suter et al., 2019;

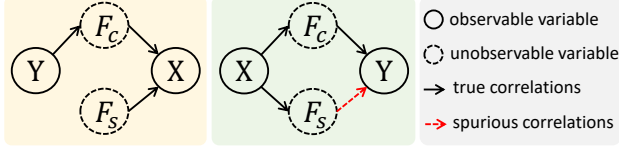


Figure 2: Structural Causal Model (SCM) for MML. **Left:** causal generating mechanism, **Right:** the learning process.

(Hu et al., 2022b), each sample is composed of various generating factors, e.g., color, shape, etc. In the context of MML, each sample contains generating factors from all modalities. From a causal perspective (Pearl, 2009), these generating factors can be divided into task-related factors that come from the label, i.e., causal factors F_c , and task-independent factors, i.e., non-causal factors F_s . The key to accurate prediction lies in extracting the causal generating factors F_c that are related to labels in the latent space (Deshpande et al., 2022). Thus, the goal of f_θ can be re-established as learning representations that contain all causal generating factors F_c from the data without F_s for accurate prediction.

Example of Causal Sufficiency and Necessity As shown in Figure 1, assume that the training data is with three modalities of image, text, and audio, and all the modalities have the feature “duck paws” when a “duck” exists. The goal of this MML task is to classify the “duck”. Then, the models that learn representations based on consistency will capture the features of “duck paws”, and can establish the label “duck” based on the learned representations. However, the learned model may also make errors in another “duck” scenario where the MML samples do not contain “duck paws”, e.g., “duck swim on the lake” (upper right in Figure 1). This suggests that the learned representation contains *sufficient but unnecessary* causes since the label “duck” can be predicted using the current representation, but may not work in another scenario. Similarly, there are some *necessary but insufficient* representations, e.g., “duck” must with “wings”, but “wings” may also correspond to another label, e.g., “bird” (lower of Figure 1). For *sufficient and necessary* causes, they ensure that the learned representations not only reflect the features target the “duck” label, e.g., “duck paws”, but also the features where the “duck” label must have, e.g., “wings”. Thus, good representations must have both causal sufficiency and necessity, i.e., causal complete causes, which is the goal we explore in this study.

Causal Analysis of MML We conduct a Structural Causal Model (SCM) for MML based on causal generating mechanism (Suter et al., 2019; Deshpande et al., 2022), as shown in Figure 2 left. In this SCM, Y and X denote the label variable and corresponding generated data variable in the MML task. F_c and F_s represent the distinct sets of generating factors that are causally and non-causally related to Y . Each generating factor corresponds to a semantic of the MML

task, e.g., color, shape, background, modality indicator, etc. Since both F_c and F_s represent high-level knowledge of the data but only F_c is causally related to Y , we could naturally define the MML task label variable Y as the cause of the F_c , i.e., $Y \rightarrow F_c$. There is no connection between F_s and Y . Following (Hu et al., 2022a; Deshpande et al., 2022), the sample in each modality is generated simultaneously using all the generating factors, including factors caused from the label and unobservable variables, e.g., environmental effects. The unobservable variable results in the generating factors F_s , which is non-causally related to Y . Then, we get both $F_c \rightarrow X$ and $F_s \rightarrow X$. Thus, we obtain Figure 2 left. Based on this, we further construct a SCM to discuss the learning process of MML, as shown in Figure 2 right. It can be viewed as the inverse process of the causal generating mechanism. Based on Figure 2 left, an ideal MML model should only utilize causal generating factors F_c and be invariant to any intervention on non-causal generating factors F_s . However, in practice, F_c and F_s in the learned representation may be coupled (Dong et al., 2024; Li et al., 2023). This leads to the model potentially learning based on non-causal F_s . There exist spurious correlations between F_s and Y , i.e., we get the additional $F_s \rightarrow Y$ in Figure 2 right.

The presence of spurious correlations leads to inaccuracies in MML. Specifically, the learned MML representations may fall into four scenarios: (i) sufficient and necessary: contains all F_c ; (ii) necessary but insufficient: contains part of F_c ; (iii) sufficient but unnecessary: contains all F_c with F_s ; (iv) insufficient and unnecessary: only contains F_s . See Appendix D and G for more analyses. To ensure accurate and robust MML, in this paper, we aim to propose a methodology that constrains the model to learn representations only contain causally sufficient and necessary information.

3. Causal Complete Cause

To access the learning of causal sufficient and necessary representations, in this section, we first provide the definition of causal sufficiency and necessity in MML, i.e., Causal Complete Cause (C^3). Next, we discuss the identifiability of C^3 , which ensures the quantification of C^3 through observable data in practice, even in corner cases (non-monotonicity and non-exogeneity). Finally, we give the measurement of C^3 , i.e., C^3 risk to measure the probability of whether the learned MML representation is causally complete.

3.1. Definition of C^3

To learn representations of causal variable F_c for MML that is with both causal sufficiency and necessity, based on (Pearl, 2009; Yang et al., 2024), we introduce the concept of the probability of Causal Complete Cause (C^3) as follows:

Definition 3.1 (Probability of Causal Complete Cause (C^3)). Denote that the data and corresponding label variables of

the given multi-modal data distribution are X and Y , while the variable of the learned MML representation is Z . Let the specific implementations of representation variable Z as c and \bar{c} , where c denotes the implementation that results in the accurate label prediction $Y = y$, and $\bar{c} \neq c$ denotes the implementation resulting in $Y \neq y$. The probability that Z is the causal complete cause of Y can be defined as:

$$C^3(Z) := \underbrace{P(Y_{do(Z=c)} = y \mid Z = \bar{c}, Y \neq y)}_{\text{Sufficiency}} P(Z = \bar{c}, Y \neq y) + \underbrace{P(Y_{do(Z=\bar{c})} \neq y \mid Z = c, Y = y)}_{\text{Necessity}} P(Z = c, Y = y), \quad (1)$$

where $P(Y_{do(Z=c)} = y \mid Z = \bar{c}, Y \neq y)$ denotes the probability of $Y = y$ when force Z to be another specific implementation c via do-operator $do(Z = c)$, when giving observations $Z = \bar{c}$ and $Y \neq y$ with probability $P(Z = \bar{c}, Y \neq y)$. Similarly, the second term corresponds to the case that where the observations are $Z = c$ and $Y = y$, the probability of Y becomes incorrect when force $Z = \bar{c}$.

Definition 3.1 indicates that when Z with a high C^3 score, it has a high probability of being the causal complete cause of Y . The two terms in Eq.1 correspond to sufficiency and necessity, respectively. Specifically, the sufficiency term $P(Y_{do(Z=c)} = y \mid Z = \bar{c}, Y \neq y)$ means that even when $Z = \bar{c}$ and $Y \neq y$, intervening to set $Z = c$ results in a high probability of $Y = y$, indicating that $Z = c$ has a sufficient causal effect on the occurrence of $Y = y$. Correspondingly, for necessity term $P(Y_{do(Z=\bar{c})} \neq y \mid Z = c, Y = y)$, even when $Z = c$ and $Y = y$, intervening to set $Z = \bar{c}$ results in $Y \neq y$, indicating that $Z = c$ is necessary for the occurrence of $Y = y$. Under this condition, the learned representation can be divided into sufficient but unnecessary causes, necessary but insufficient causes, sufficient and necessary causes, and insufficient and unnecessary causes (**Appendix D** for detailed analyses). We aim to constrain the C^3 score of the learned representation, i.e., extract sufficient and necessary causes, to achieve robust and accurate MML.

3.2. Identifiability of C^3

Since it is difficult to obtain all samples in the multi-modal data distribution, especially in real systems, e.g., the counterfactual data in the definition of C^3 is difficult to obtain (Kusner et al., 2017; Morgan & Winship, 2015), calculating the probability of C^3 is still a challenging issue. To access the calculation of C^3 based on observable MML data, we discuss the identifiability of C^3 in this section.

Identifiability refers to the ability to uniquely infer causal effects from observable data under given assumptions (Pearl, 2009). For MML settings, it means the causal factors within the representation Z can uniquely determine the label Y

from the sample X . To ensure reliable estimation, we constrain the C^3 score of the learned representation Z extracted from X , ensuring its identifiability. In previous studies (Tian & Pearl, 2002; Yang et al., 2024), identifying causal probabilities typically assumes that statistical data are derived under exogeneity and monotonicity conditions (**Definition D.1** and **Definition D.2** in **Appendix D.4**). Exogeneity refers to where the external intervention’s impact on the conditional distribution $P(Y|Z)$ is negligible when the variable Z is exogenous to Y . This ensures the learned Z to recognize F_c without being affected by F_s . Monotonicity, on the other hand, describes the consistent, unidirectional effect of the representation Z on Y . This ensures that the impact of the learned representation Z on the labeling decision will not be reversed as other factors change. However, in practice, non-trivial cases often arise: the inseparability of generating factors in the latent space leads to spurious correlations, i.e., the learned representations contain non-causal F_s (**Figure 2**); Meanwhile, modality conflicts and the high-dimensional nonlinear interactions (Wang et al., 2023d; Huang et al., 2021b) undermine monotonicity. These challenges render traditional identifiability conditions inapplicable. To address this, we relax the above assumptions and explore the identifiability of C^3 , accessing the calculation of C^3 score.

Consider the effects of spurious correlations, i.e., $P(Y_{do(Z=c)}) \neq P(Y \mid Z = c)$, we first relax the exogeneity assumption. Based on **Definition 3.1**, we extend Theorem 9.2.15 in (Pearl, 2009) to MML for C^3 , obtaining:

Theorem 3.2 (Identifiability under Non-Exogeneity). *Given the MML model f_θ , where the label variable Y is influenced by the causal factors F_c and non-causal factors F_s . Assume f_θ satisfy the Positive Markovian assumption (Tian & Pearl, 2002), the probabilities of C^3 ($P(Y_{do(Z=c)} = y, Y_{do(Z=\bar{c})} \neq y)$) is identifiable and can be estimated via:*

$$C^3(Z) = P(Y_{do(Z=c)}) - P(Y_{do(Z=\bar{c})}) \quad (2)$$

where Y is monotonic relative to Z with $Y_{do(Z=c)} = \bar{y} \wedge Y_{do(Z=\bar{c})} = y$ is false or $Y_{do(Z=\bar{c})} = y \wedge Y_{do(Z=c)} = \bar{y}$ is false, and the model f_θ satisfies local invertibility.

Theorem 3.2 establishes that, under the monotonicity condition, C^3 can be estimated using observable multi-modal data, thereby quantifying C^3 . Specifically, by modeling the effects of spurious correlations (F_s on Y) as non-causal pathways in the SCM, interventions with the do-operator, such as $P(Y_{do(Z=c)})$ and $P(Y_{do(Z=\bar{c})})$, facilitates reliable causal effect estimation. For counterfactual terms ($Z = \bar{c}$) involved in the necessity probability, the model f_θ imposes locally reversible constraints to ensure identifiability, as discussed in (Galles & Pearl, 1998). Under these conditions, the probability of causal sufficiency C_{su}^3 and the probability of causal necessity C_{ne}^3 can be estimated as follows:

$$C_{su}^3(Z) = \frac{P(Y_{do(Z=c)}) - P(Y_{do(Z=\bar{c})})}{1 - P(Z=c)} \quad (3)$$

$$C_{ne}^3(Z) = \frac{P(Y_{do(Z=c)}) - P(Y_{do(Z=\bar{c})})}{P(Z=c)} \quad (4)$$

Next, according to the second paragraph of **Subsection 3.2**, considering the cross-modal conflicts with high-dimensional nonlinear interactions in practice, we relax the assumptions of monotonicity. The key idea lies in introducing an instrumental variable V (Caner & Hansen, 2004) to estimate the piecewise effects of conditional distributions within the C^3 definition. Meanwhile, V satisfies $V \perp\!\!\!\perp F_s$ with a controllable impact on F_c , i.e., $V \rightarrow F_c \rightarrow Y$. Then, we have:

Theorem 3.3 (Identifiability under Non-Monotonicity and Non-Exogeneity). *Given a model f_θ that learns the causal effect $Z \rightarrow Y$. The representation variable $Z = \Xi_c F_c + \Xi_s F_s$ where $\Xi_{(\cdot)}$ is the weight matrix. Introducing an instrumental variable V satisfying $P(Y | Z, V) \approx P(Y | Z)$, we have:*

$$C^3(Z) = \int_v [P(Y = y | Z = c, V = v) - P(Y = y | Z = \bar{c}, V = v)] P(V = v) dv. \quad (5)$$

Theorem 3.3 posits that the estimation of C^3 is achievable without the dependence on exogeneity and monotonicity, enabling the quantification of C^3 in the absence of counterfactual data. The detailed discussion is provided in **Appendix D.4**, and the proofs of the above theorems are provided in **Appendix A.1 and A.2**, respectively. According to this theorem, the practical estimation of C^3 hinges on how the instrumental variable V is modeled and how the sufficiency and necessity terms of C^3 are constrained under V , also the main focus in the next subsection, i.e., measurement of C^3 .

3.3. Measurement of C^3

Based on **Definition 3.1** and **Theorem 3.3**, we provide the measurement of C^3 in this section, i.e., C^3 risk, to estimate the C^3 score of the representation distribution $P(Z|X = x)$ inferred from X on the multi-modal data distribution P_{XY} . When the learned representation obtains less necessary and sufficient information, the C^3 risk will be higher. Specifically, we first model the instrumental variable V based on **Theorem 3.3**. It aims to make the MML model learn representations Z that only contain the causal factors F_c for decision-making while ensuring the identifiability of the C^3 score assessment (**Theorem 3.4**). Next, based on **Definition 3.1**, we provide the C^3 measurement of the learned Z , i.e., C^3 risk (**Theorem 3.5**). We employ a twin network (**Figure 5**) with a real-world branch (extract causal representation using the proposed instrumental variable) and a hypothetical-world branch (modeling counterfactual data with gradient-based adjustments), thereby modeling the sufficiency and necessity terms. **Appendix D.5** establishes the reliability of the proposed twin network.

Firstly, as shown in **Section 2**, we establish the model f_θ using the feature extractor g and the linear classifier

$\mathcal{W} : \mathbb{R}^d \rightarrow \mathcal{Y}$ on the overall representation $Z = g(X)$ ($Z = \Xi_c F_c + \Xi_s F_s$) to obtain the label $Y = \text{sign}(\mathcal{W}^\top g(X))$. To infer F_c from observable data $x \sim \mathcal{X}$, we use the instrumental variable V . Here, we focus on how V is modeled to constrain Z only contains F_c for decision-making while satisfying the conditions in **Theorem 3.3**. We propose:

Theorem 3.4 (Instrumental Variable V in MML). *For multimodal input $X \in \mathbb{R}^{K \times d}$, representing K modalities each with a feature dimension of d , instrumental variable V is introduced to extract causal generating factors F_c while reducing the influence of non-causal factors F_s . V is generated from X using self-attention mechanism with:*

$$V = \sum_{j=1}^K \frac{\exp(s_{ij})}{\sum_{k=1}^K \exp(s_{ik})} X_j W_V, \quad (6)$$

where $s_{ij} = \frac{q_i^\top k_j}{\sqrt{d}} - \alpha \|q_i - k_j\|^2$.

where $q_i = X_i W_Q$ and $k_j = X_j W_K$ are the query and key of i -th and j -th modalities' features, $W_Q, W_K, W_V \in \mathbb{R}^{d \times d}$ are linear projection matrices, mapping query, key and value respectively. Then, V satisfies (i) $P(Z | V) \neq P(Z)$; (ii) $P(F_s | V) = P(F_s)$; and (iii) $P(Y | Z, V) = P(Y | F_c)$.

In **Theorem 3.4**, we propose using the self-attention mechanism to model the instrumental variable V for C^3 . Specifically, the alignment scores s_{ij} is to capture inter-modal interactions for label. Then, by strengthening the correlation between V and Z , the learned representation Z is guided to approach F_c while weakening the correlation with F_s . Furthermore, consider inter-modal misalignment, $\|q_i - k_j\|^2$ with weight α is introduced as a distance-based adjustment to diminish the impact of modalities with large feature distances on attention weights. It satisfies three conditions: (i) Relevance: V manipulate F_c ; (ii) Independence: V is conditionally independent from F_s ; and (iii) Exclusion: the influence of V on Y is completely indirectly realized through F_c . The detailed proofs are provided in **Appendix A.3**.

Next, based on these results, we provide the measurement of C^3 , i.e., C^3 risk. Specifically, we first utilize V to constrain f_θ , effectively distinguishing F_c from F_s and ensuring the identifiability of C^3 based on **Theorem 3.4**. Obtaining Z_c that only contains F_c , we then define sufficiency risk (when $Z = c$, the label is not y) and necessity risk (when $Z = \bar{c}$, the label is y) to construct the C^3 risk based on **Definition 3.1** and Eq.5. The key challenge lies in the counterfactual data, i.e., $\bar{Z}_c : Z = \bar{c}$, is difficult to obtain (Kusner et al., 2017; Morgan & Winship, 2015). To address this, we propose a twin network comprising: (i) the real-world branch to obtain \hat{Z}_c with V , and (ii) the hypothetical-world branch to obtain \bar{Z}_c under a provable gradient-based adjustment, ensuring \bar{Z}_c stay close to the original observable distribution (**Appendix D.5**). These branches share network structures

and parameters, maintaining a mirrored correspondence that enforces causal consistency (Pearl, 2009). Thus, we get:

Theorem 3.5 (C^3 Risk). *Given N observable samples $\{(x_i, y_i)\}_{i=1}^N$ drawn from the multi-modal distribution P_{XY} , and the model f_θ with feature extractor $g(\cdot)$ and linear classifier \mathcal{W} , we define the following twin-network:*

$$\begin{aligned} \hat{Z}_{c,i} &= g^*(x_i, v_i), \quad \bar{Z}_{c,i} = \hat{Z}_{c,i} + \Delta_i, \\ \text{where } \Delta_i &= -\nabla_{\bar{Z}_{c,i}} \ell\left(\sigma(\mathcal{W}^\top \bar{Z}_{c,i}), y_i\right), \\ \text{s.t. } \mu_{KL}(\bar{Z}_{c,i}, \hat{Z}_{c,i}) &\leq \varepsilon, \quad \forall i, \end{aligned} \quad (7)$$

where $g^*(x_i, v_i)$ is the calibrated g with v_i using Kullback-Leibler divergence $\mu_{KL}(\cdot)$, i.e., with loss $\mathcal{L}_v = \mathbb{E}_{(x,y) \sim P_{XY}} \mathbb{E}_{v_i \in V} \mu_{KL}(g(x), v_i)$, to estimate the causal representation $\hat{Z}_{c,i}$ in the real-world branch, Δ_i arises from the gradient-based intervention with $v_i \sim V$ for the hypothetical world. If f_θ converges to an optimal solution under a Monte Carlo approximation of V , then by using:

$$\hat{R}^{C^3} = \frac{1}{N} \sum_{i=1}^N \left[\rho[\sigma(\mathcal{W}^\top \hat{Z}_{c,i}) \neq y_i] + \rho[\sigma(\mathcal{W}^\top \bar{Z}_{c,i}) = y_i] \right], \quad (8)$$

the discrepancy between $\hat{R}_N^{C^3}$ and the ideal causal complete quantity approaches zero with high probability. Here, σ denotes the signum function, $\rho(\cdot)$ denotes an indicator function which is equal to 1 if the condition in $\rho(\cdot)$ is true.

Theorem 3.5 presents a method to measure the causal completeness of learned representations based on observable data. It leverages instrumental variables V and a twin network to address the issues of spurious correlations in MML and the unavailability of counterfactual data in practice. The detailed proofs and analysis are provided in **Appendix A.4**.

4. Performance Guarantee with C^3 Risk

In this section, we conduct theoretical analyses to establish the connection between the proposed C^3 risk and MML generalization performance, proving its effectiveness.

Before discussing generalization, we first illustrate the empirical and expectation risks of the MML model f_θ on training and test data, i.e., $\hat{R}^{C^3}(f_\theta)$ (Eq.8) and $R^{C^3}(f_\theta) = \mathbb{E}_{(x,y) \sim P_{XY}} \rho[\sigma(\mathcal{W}^\top \hat{F}_{c,i}) \neq y_i] + \rho[\sigma(\mathcal{W}^\top \bar{F}_{c,i}) = y_i]$. Then, we provide the following performance guarantee:

Theorem 4.1 (Performance Guarantee via C^3). *Denote the hypothesis set \mathcal{H} of linear classifier $\mathcal{W} \in \mathcal{H} \subseteq \{h : \mathbb{R}^d \rightarrow \mathcal{Y}\}$, let $H = \text{Pdim}(\{\ell_h : h \in \mathcal{H}\})$. Then with probability at least $1 - \delta$, and training samples that sampling from empirical distribution $\mathcal{D}_{tr}(x, y)$, we have*

$$R^{C^3}(f_\theta) \leq \hat{R}^{C^3}(f_\theta) + M\mathfrak{R}(\mathcal{H}) + \sqrt{\frac{\ln(1/\delta)}{2H}}. \quad (9)$$

Here, $\mathfrak{R}(H)$ is the Rademacher complexity of the hypothesis class H , and M is a finite constant.

Theorem 4.1 derives the upper bound on the generalization error of C^3 risk, relating its empirical error on the training data to its performance on unseen samples. Specifically, the generalization error is bounded by the sum of the empirical error, the Rademacher complexity of the hypothesis class of linear classifier, and a confidence term that controls the probability of exceeding the bound. This result provides a theoretical performance guarantee for optimizing MML models with C^3 risk. See **Appendix A.5** for detailed proofs.

5. Learning Causal Complete Representations

Based on the above theoretical results, we propose a plug-and-play method, Causal Complete Cause Regularization (C^3R), which is built upon the C^3 risk to extract causal complete representations from observable multi-modal data.

Specifically, we first introduce the constraints of the instrumental variable V (**Theorem 3.4**) to make the MML model f_θ learn causal representations while satisfying the identifiability in practice. Then, we minimize the C^3 risk of the learned representations (**Theorem 3.5**) to ensure the causal completeness of the learned representation, i.e., causal sufficiency and necessity. In summary, the objective of C^3R is a combination of the above two-step objectives, which can be embedded in various MML models. It can be expressed as:

$$\min_{f_\theta} \hat{R}^{C^3} + \lambda_v \mathcal{L}_v + \lambda_{fe} \mathcal{L}_{fe} \quad (10)$$

where λ_v and λ_{fe} denotes the importance weights, the three terms: (i) \hat{R}^{C^3} (Eq.8) constrains the model to learn a causally complete representation, i.e., one that exhibits minimal sufficiency and necessity risk; (ii) \mathcal{L}_v , built upon **Theorem 3.4**, employs the instrumental variable V to guide the model toward the causal representation, corresponding to the real-world branch; (iii) \mathcal{L}_{fe} stems from the counterfactual construction condition in Eq. 7, specifically $\mathcal{L}_{fe} = \frac{1}{N} \sum_{i=1}^N \mu_{KL}(\bar{Z}_{c,i}, \hat{Z}_{c,i})$, ensuring that $\hat{Z}_{c,i}$ remains within the feasible region. Thus, by minimizing the above objective, the C^3 score of the learned representation will be higher while maintaining the required conditions for practical implementations. Then, it makes the learned representation causally sufficient and necessary with high confidence.

6. Experiments

In this section, we conduct extensive experiments on various benchmark datasets to verify the effectiveness of C^3R . More details and experiments are provided in **Appendix E-H**.

6.1. Experimental Settings

Datasets We select six datasets: (i) scenes recognition on NYU Depth V2 (Silberman et al., 2012) and SUN RGBD (Song et al., 2015) with RGB and depth images; (ii) image-

Table 1: Performance comparison when 50% samples are corrupted with Gaussian noise i.e., zero mean with the variance of N . “(N, Avg.)” and “(N, Worst.)” denotes the average and worst-case accuracy. The best results are highlighted in **bold**.

Method	NYU Depth V2				SUN RGB-D				FOOD 101				MVSA			
	(0,Avg.)	(0,Worst.)	(10,Avg.)	(10,Worst.)	(0,Avg.)	(0,Worst.)	(10,Avg.)	(10,Worst.)	(0,Avg.)	(0,Worst.)	(10,Avg.)	(10,Worst.)	(0,Avg.)	(0,Worst.)	(10,Avg.)	(10,Worst.)
CLIP (Sun et al., 2023)	69.32	68.29	51.67	48.54	56.24	54.73	35.65	32.76	85.24	84.20	52.12	49.31	62.48	61.22	31.64	28.27
ALIGN (Jia et al., 2021)	66.43	64.33	45.24	42.42	57.32	56.26	38.43	35.13	86.14	85.00	53.21	50.85	63.25	62.69	30.55	26.44
MaPLe (Khattak et al., 2023)	71.26	69.27	52.98	48.73	62.44	61.76	34.51	30.29	90.40	86.28	53.16	40.21	77.43	75.36	43.72	38.82
CoOp (Jia et al., 2022a)	67.48	66.94	49.43	45.62	58.36	56.31	39.67	35.43	88.33	85.10	55.24	51.01	74.26	73.61	42.58	37.29
VPT (Jia et al., 2022a)	62.16	61.21	41.05	37.81	54.72	53.92	33.48	29.81	83.89	82.00	51.44	49.01	65.87	64.98	32.79	29.21
Late fusion (Wang et al., 2016)	69.14	68.35	51.99	44.95	62.09	60.55	47.33	44.60	90.69	90.58	58.00	55.77	76.88	74.76	55.16	47.78
ConcatMML (Zhang et al., 2021)	70.30	69.42	53.20	47.71	61.90	61.19	45.64	42.95	89.43	88.79	56.02	54.33	75.42	75.33	53.42	50.47
AlignMML (Wang et al., 2016)	70.31	68.50	51.74	44.19	61.12	60.12	44.19	38.12	88.26	88.11	55.47	52.76	74.91	72.97	52.71	47.03
ConcatBow (Zhang et al., 2023c)	49.64	48.66	31.43	29.87	41.25	40.54	26.76	24.27	70.77	70.68	35.68	34.92	64.09	62.04	45.40	40.95
ConcatBERT (Zhang et al., 2023c)	70.56	69.83	44.52	43.29	59.76	58.92	45.85	41.76	88.20	87.81	49.86	47.79	65.59	64.74	46.12	41.81
MMTM (Joze et al., 2020)	71.04	70.18	52.28	46.18	61.72	60.94	46.03	44.28	89.75	89.43	57.91	54.98	74.24	73.55	54.63	49.72
TMC (Han et al., 2020)	71.06	69.57	53.36	49.23	60.68	60.31	45.66	41.60	89.86	89.80	61.37	61.10	74.88	71.10	60.36	53.37
LCKD (Wang et al., 2023b)	68.01	66.15	42.31	40.56	56.43	56.32	43.21	42.43	85.32	84.26	47.43	44.22	62.44	62.27	43.52	38.63
UniCODE (Xia et al., 2024)	70.12	68.74	44.78	42.79	59.21	58.55	46.32	42.21	88.39	87.21	51.28	47.95	66.97	65.94	48.34	42.95
SimMMDG (Dong et al., 2024)	71.34	70.29	45.67	44.83	60.54	60.31	47.86	45.79	89.57	88.43	52.55	50.31	67.08	66.35	49.52	44.01
MMBT (Kiela et al., 2019)	67.00	65.84	49.59	47.24	56.91	56.18	43.28	39.46	91.52	91.38	56.75	56.21	78.50	78.04	55.35	52.22
QMF (Zhang et al., 2023c)	70.09	68.81	55.60	51.07	62.09	61.30	48.58	47.50	92.92	92.72	62.21	61.76	78.07	76.30	61.28	57.61
CLIP+ C^3R	76.54	75.12	56.73	52.90	62.31	58.71	41.59	37.52	92.93	91.80	59.77	57.54	69.61	68.64	39.58	35.89
MaPLe+ C^3R	77.07	74.45	58.94	55.95	66.21	65.51	40.12	37.34	94.38	93.51	60.63	46.07	81.19	81.51	49.32	45.98
Late fusion+ C^3R	73.26	71.62	57.21	50.98	64.84	63.25	53.35	50.43	94.09	92.24	65.27	59.02	83.77	79.79	62.14	52.50
LCKD+ C^3R	77.14	75.12	50.11	47.98	60.97	60.14	47.23	46.21	90.89	90.14	54.48	51.16	66.78	65.67	49.28	42.84
SimMMDG+ C^3R	75.32	74.61	49.99	47.22	65.50	64.58	52.69	51.70	92.24	91.14	57.32	53.56	73.62	71.01	51.65	51.07
MMBT+ C^3R	73.74	71.82	54.35	52.57	61.47	59.99	48.42	46.07	94.25	93.90	60.41	60.11	82.76	81.64	62.12	58.93
QMF+ C^3R	77.58	74.95	59.72	59.18	67.35	65.84	52.26	51.28	94.87	93.79	66.45	63.69	83.13	81.98	66.66	64.51

Table 2: Performance with missing modalities on BraTS. The brackets “()” indicate the effect changes after introducing C^3R . “●” and “○” indicate the availability and absence of the modality for testing. The best results are highlighted in **bold**.

Modalities				Enhancing Tumour							Tumour Core							Whole Tumour						
Fl	T1	T1c	T2	HMIS	HVED	RSeg	mmFm	LCKD	LCKD+C ³ R	HMIS	HVED	RSeg	mmFm	LCKD	LCKD+C ³ R	HMIS	HVED	RSeg	mmFm	LCKD	LCKD+C ³ R			
●	○	○	○	11.78	23.80	25.69	39.33	45.48	49.81 (+4.33)	26.06	57.90	53.57	61.21	72.01	76.65 (+4.64)	52.48	84.39	85.69	86.10	89.45	91.62 (+2.17)			
○	●	○	○	10.16	8.60	17.29	32.53	43.22	49.13 (+6.01)	37.39	33.90	47.90	56.55	66.58	72.18 (+5.60)	57.62	49.51	70.11	67.52	76.48	82.39 (+5.91)			
○	○	●	○	62.02	57.64	67.07	72.60	75.65	80.50 (+4.85)	65.29	59.59	76.83	75.41	83.02	88.06 (+5.04)	61.53	53.62	73.31	72.22	77.23	81.93 (+4.70)			
○	○	○	●	25.63	22.82	28.97	43.05	47.19	54.13 (+6.94)	57.20	54.67	57.49	64.20	70.17	77.32 (+7.15)	80.96	79.83	82.24	81.15	84.37	90.78 (+6.41)			
●	●	○	○	10.71	27.96	32.13	42.96	48.30	54.16 (+4.86)	41.12	61.14	60.68	65.91	74.58	79.83 (+5.25)	64.62	85.71	88.24	87.06	89.97	93.63 (+3.66)			
●	○	○	○	66.10	68.36	70.30	75.07	78.75	82.98 (+4.23)	71.49	75.07	80.62	77.88	85.67	89.74 (+4.07)	68.99	85.93	88.51	87.30	90.47	93.91 (+3.44)			
●	○	○	●	30.22	32.31	33.84	47.52	49.01	56.12 (+7.11)	57.68	62.70	61.16	69.75	75.41	82.57 (+7.16)	82.95	87.58	88.28	87.59	90.39	95.48 (+5.09)			
○	●	○	○	66.22	61.11	69.06	74.04	76.09	81.76 (+5.67)	72.46	67.55	78.72	78.59	82.49	88.32 (+5.83)	68.47	64.22	77.18	74.42	80.10	87.03 (+6.96)			
○	○	○	●	32.39	24.29	32.01	44.99	50.09	56.03 (+5.94)	60.92	56.26	62.19	69.42	72.75	78.78 (+6.03)	82.41	81.56	84.78	82.20	86.05	92.33 (+6.28)			
○	○	○	●	67.83	67.83	69.71	74.51	76.01	83.97 (+7.96)	76.64	73.92	80.20	78.61	84.85	93.57 (+8.72)	82.48	81.32	85.19	82.99	86.49	94.40 (+7.91)			
●	○	○	○	68.54	68.60	70.78	75.47	77.78	82.94 (+5.06)	76.01	77.05	81.06	79.80	85.24	90.46 (+5.22)	72.31	86.72	88.73	87.33	90.50	95.51 (+5.01)			
●	○	○	○	31.07	32.34	36.41	47.70	49.96	56.25 (+6.29)	60.32	63.14	64.38	71.52	76.68	82.69 (+6.01)	83.43	88.07	88.81	87.75	90.46	96.23 (+5.77)			
○	○	○	○	68.72	68.93	70.88	75.67	77.48	83.90 (+6.42)	77.53	76.75	80.72	79.55	85.56	92.39 (+6.83)	83.85	88.09	89.27	88.14	90.90	96.78 (+5.88)			
○	○	○	○	69.92	67.75	70.10	74.75	77.60	82.54 (+4.94)	78.96	75.28	80.33	80.39	84.02	89.43 (+5.41)	83.94	82.32	86.01	82.71	86.73	91.73 (+5.00)			
●	○	○	○	70.24	69.03	71.13	77.61	79.33	86.36 (+7.03)	79.48	77.71	80.86	85.78	85.31	91.43 (+6.12)	84.74	88.46	89.45	89.64	90.84	95.41 (+4.57)			

text classification on UPMC FOOD101 (Wang et al., 2015) and MVSA (Niu et al., 2016) with image and text; (iii) segmentation considering missing modalities on BraTS (Menze et al., 2014; Bakas et al., 2018) with Flair, T1, T1c, and T2; and (iv) synthetic MMLSynData (see Appendix D.1).

Implementation Details We use a three-layer MLP with activation functions (Clevert et al., 2015) as the representation learner. The hidden vector dimensions of each layer are specified as 64, 32, and 128, while the learned representation is 64. For optimization, we employ the Adam optimizer (Kingma & Ba, 2014) with Momentum and weight decay set at 0.8 and 10^{-4} . The initial learning rate is established at 0.1, with the flexibility for linear scaling as required. Additionally, we use grid search to set the hyperparameters $\lambda_v = 0.75$ and $\lambda_{fe} = 0.4$. All experimental procedures are executed in five runs via NVIDIA RTX A6000 GPUs.

6.2. Results

Performance and robustness analysis To evaluate the effectiveness of C^3R , we record the average and worst-case accuracy of various MML baselines and introduce C^3R under Gaussian noise (for image modality) and blank noise (for text modality) following (Han et al., 2020; Zhang et al., 2023d; Ma et al., 2021). The results are shown in Table 1. We can observe that C^3R achieves stable improvements in both the average and worst-case accuracy. This proves the superior effectiveness and robustness of C^3R .

When faces the problem of missing modalities Considering the missing modality issues, we evaluate the performance of C^3R and several strong baselines (Wang et al., 2023b; Bakas et al., 2018; Zhang et al., 2022) on all 15 possible combinations of missing modalities on BraTS. From Table 2, we can observe that (i) C^3R brings significant per-

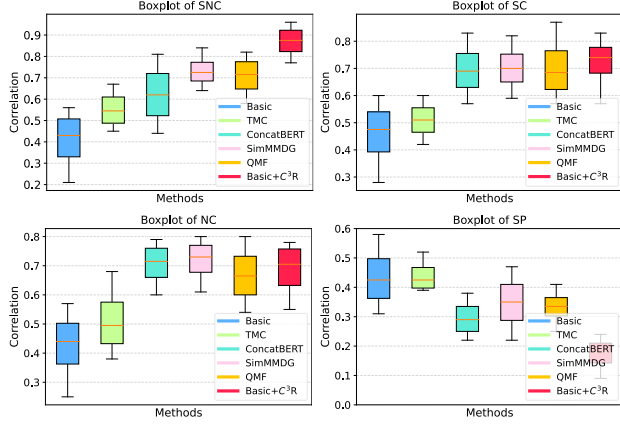


Figure 3: Evaluation for the property of learned representations (SNC, SC, NC, and SP). See **Appendix H** for details.

formance improvements; (ii) C^3R can reduce the learning gap for the representations on different modal semantics, i.e., reducing the accuracy gap of learning on the difficult-to-identify F1 and T1 modalities and the easy T1c. This demonstrates the superiority of C^3R and the advantage of causally complete representation in missing modality issues.

Learning causal complete representations To evaluate C^3R 's ability to extract causal complete causes, we conduct experiments: (i) construct four types of MML data, i.e., sufficient and necessary (SNC), sufficient but unnecessary (SC), necessary but insufficient causes (NC), and spurious correlations (SP) following (Yang et al., 2024) (see **Appendix H** for more details); then (ii) evaluate their correlation with the learned representation based on the distance metric (Jones et al., 1995), i.e., the higher the score, the stronger the correlation. The results are shown in **Figure 3** (see **Appendix D** and **H** for details). The representations learned by C^3R have a higher correlation with SNC and lower with SP. This proves that C^3R can learn causal complete representations more effectively while other methods are hard to achieve.

Ablation Study To evaluate the effect of each item in C^3R (Eq.10), we evaluate the performance change on LCKD+ C^3R . We consider the standard and corner case (missing modality), and conduct experiments on FOOD 101 and BraTS, as shown in **Figure 4**. We can observe that each item plays an important role. See **Appendix H** for more experiments, e.g., model efficiency and parameter sensitivity.

7. Related Work

Multi-modal learning aims to learn good representations through multiple modalities for accurate prediction. Recently, multiple methods (Xu et al., 2023; Jia et al., 2022b; Wang et al., 2023c; Fan et al., 2024) have been proposed to solve MML tasks through modality consistency, e.g., tokenize diverse modalities into sequences and utilize Trans-

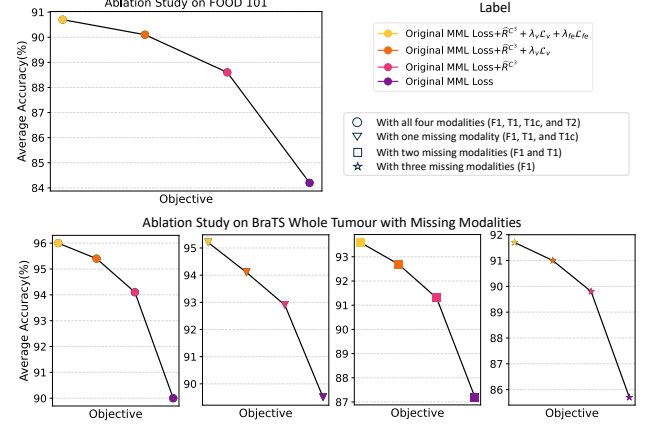


Figure 4: Ablation study of C^3R (performance when removing different regular terms). See **Appendix H** for details.

formers for joint learning (Bao et al., 2022; Wang et al., 2022), whereas CLIP (Radford et al., 2021; Fan et al., 2024), ALIGN (Jia et al., 2021), etc. employ distinct encoders for each modality and utilize contrastive loss to synchronize features. These methods align features from different modalities into the same space to capture the primary events. Another type of work (Jiang et al., 2023; Dong et al., 2024; Wang et al., 2023a; Wu et al., 2020) proposed to additionally focus on modality specificity. They divide the MML features into modality-shared and modality-specific components and learn separately. However, all these methods may result in learning insufficient or unnecessary information. Meanwhile, they rely on strong assumptions like semantic alignment (Akbari et al., 2021; Wang et al., 2023c; Lu et al., 2022; Zhang et al., 2023b) and may be limited to ideal data (Ge et al., 2023; Zhang et al., 2023a), affecting model performance. For causal sufficiency and necessity, (Pearl, 2009) first proposed the related concepts, and (Yang et al., 2024) applied it to domain generalization with assumptions in an ideal environment. The differences between our methodology and theirs include problem settings, theorems, implementations, learning objectives, etc. (See **Appendix D.6** for detailed comparison). We explore the MML-specific concepts of causal completeness without strong assumptions, ensuring the effectiveness of the learned representations.

8. Conclusion

We explore the MML-specific concepts of causal sufficient and necessary without exogeneity and monotonicity assumptions. To measure whether the learned MML representation is causally complete, we present the definition, identifiability, and measurement of C^3 with theoretical support. Based on these results, we propose a plug-and-play method C^3R to promote MML learning causal complete representations. Extensive experiments demonstrate its effectiveness.

Impact Statement

This paper presents work whose goal is to advance the field of Machine Learning and Multi-Modal Learning. There are many potential societal consequences of our work, none of which we feel must be specifically highlighted here.

References

- Abdollahzadeh, M., Malekzadeh, T., and Cheung, N.-M. M. Revisit multimodal meta-learning through the lens of multi-task learning. *Advances in Neural Information Processing Systems*, 34:14632–14644, 2021.
- Ahuja, K., Shanmugam, K., Varshney, K., and Dhurandhar, A. Invariant risk minimization games. In *International Conference on Machine Learning*, pp. 145–155. PMLR, 2020.
- Akbari, H., Yuan, L., Qian, R., Chuang, W.-H., Chang, S.-F., Cui, Y., and Gong, B. Vatt: Transformers for multimodal self-supervised learning from raw video, audio and text. *Advances in Neural Information Processing Systems*, 34: 24206–24221, 2021.
- Bakas, S., Reyes, M., Jakab, A., Bauer, S., Rempfler, M., Crimi, A., Shinohara, R. T., Berger, C., Ha, S. M., Rozycki, M., et al. Identifying the best machine learning algorithms for brain tumor segmentation, progression assessment, and overall survival prediction in the brats challenge. *arXiv preprint arXiv:1811.02629*, 2018.
- Baltrušaitis, T., Ahuja, C., and Morency, L.-P. Multimodal machine learning: A survey and taxonomy. *IEEE transactions on pattern analysis and machine intelligence*, 41 (2):423–443, 2018.
- Bao, H., Wang, W., Dong, L., Liu, Q., Mohammed, O. K., Aggarwal, K., Som, S., Piao, S., and Wei, F. Vlmo: Unified vision-language pre-training with mixture-of-modality-experts. *Advances in Neural Information Processing Systems*, 35:32897–32912, 2022.
- Caner, M. and Hansen, B. E. Instrumental variable estimation of a threshold model. *Econometric theory*, 20(5): 813–843, 2004.
- Clevert, D.-A., Unterthiner, T., and Hochreiter, S. Fast and accurate deep network learning by exponential linear units (elus). *arXiv preprint arXiv:1511.07289*, 2015.
- Deshpande, S., Wang, K., Sreenivas, D., Li, Z., and Kuleshov, V. Deep multi-modal structural equations for causal effect estimation with unstructured proxies. *Advances in Neural Information Processing Systems*, 35: 10931–10944, 2022.
- Dong, H., Nejjar, I., Sun, H., Chatzi, E., and Fink, O. Simmdg: A simple and effective framework for multi-modal domain generalization. *Advances in Neural Information Processing Systems*, 36, 2024.
- Fan, L., Krishnan, D., Isola, P., Katabi, D., and Tian, Y. Improving clip training with language rewrites. *Advances in Neural Information Processing Systems*, 36, 2024.
- Frost, R., Armstrong, B. C., Siegelman, N., and Christiansen, M. H. Domain generality versus modality specificity: The paradox of statistical learning. *Trends in cognitive sciences*, 19(3):117–125, 2015.
- Galles, D. and Pearl, J. An axiomatic characterization of causal counterfactuals. *Foundations of Science*, 3:151–182, 1998.
- Ge, Y., Ren, J., Gallagher, A., Wang, Y., Yang, M.-H., Adam, H., Itti, L., Lakshminarayanan, B., and Zhao, J. Improving zero-shot generalization and robustness of multi-modal models. In *Proceedings of the IEEE/CVF Conference on Computer Vision and Pattern Recognition*, pp. 11093–11101, 2023.
- Han, Z., Zhang, C., Fu, H., and Zhou, J. T. Trusted multi-view classification. In *International Conference on Learning Representations*, 2020.
- Hu, L., Chen, Z., Zhao, Z., Yin, J., and Nie, L. Causal inference for leveraging image-text matching bias in multi-modal fake news detection. *IEEE Transactions on Knowledge and Data Engineering*, 35(11):11141–11152, 2022a.
- Hu, Z., Zhao, Z., Yi, X., Yao, T., Hong, L., Sun, Y., and Chi, E. Improving multi-task generalization via regularizing spurious correlation. *Advances in Neural Information Processing Systems*, 35:11450–11466, 2022b.
- Huang, Y., Du, C., Xue, Z., Chen, X., Zhao, H., and Huang, L. What makes multi-modal learning better than single (provably). *Advances in Neural Information Processing Systems*, 34:10944–10956, 2021a.
- Huang, Z., Niu, G., Liu, X., Ding, W., Xiao, X., Wu, H., and Peng, X. Learning with noisy correspondence for cross-modal matching. *Advances in Neural Information Processing Systems*, 34:29406–29419, 2021b.
- Jia, C., Yang, Y., Xia, Y., Chen, Y.-T., Parekh, Z., Pham, H., Le, Q., Sung, Y.-H., Li, Z., and Duerig, T. Scaling up visual and vision-language representation learning with noisy text supervision. In *International conference on machine learning*, pp. 4904–4916. PMLR, 2021.
- Jia, M., Tang, L., Chen, B.-C., Cardie, C., Belongie, S., Hariharan, B., and Lim, S.-N. Visual prompt tuning. In

- European Conference on Computer Vision*, pp. 709–727. Springer, 2022a.
- Jia, Z., Cai, X., and Jiao, Z. Multi-modal physiological signals based squeeze-and-excitation network with domain adversarial learning for sleep staging. *IEEE Sensors Journal*, 22(4):3464–3471, 2022b.
- Jiang, Q., Chen, C., Zhao, H., Chen, L., Ping, Q., Tran, S. D., Xu, Y., Zeng, B., and Chilimbi, T. Understanding and constructing latent modality structures in multi-modal representation learning. In *Proceedings of the IEEE/CVF Conference on Computer Vision and Pattern Recognition*, pp. 7661–7671, 2023.
- Jones, T., Forrest, S., et al. Fitness distance correlation as a measure of problem difficulty for genetic algorithms. In *ICGA*, volume 95, pp. 184–192, 1995.
- Jordan, M. I. and Mitchell, T. M. Machine learning: Trends, perspectives, and prospects. *Science*, 349(6245):255–260, 2015.
- Joze, H. R. V., Shaban, A., Iuzzolino, M. L., and Koishida, K. Mmtm: Multimodal transfer module for cnn fusion. In *Proceedings of the IEEE/CVF conference on computer vision and pattern recognition*, pp. 13289–13299, 2020.
- Khattak, M. U., Rasheed, H., Maaz, M., Khan, S., and Khan, F. S. Maple: Multi-modal prompt learning. In *Proceedings of the IEEE/CVF Conference on Computer Vision and Pattern Recognition*, pp. 19113–19122, 2023.
- Kiela, D., Bhooshan, S., Firooz, H., Perez, E., and Testugine, D. Supervised multimodal bitransformers for classifying images and text. *arXiv preprint arXiv:1909.02950*, 2019.
- Kingma, D. P. and Ba, J. Adam: A method for stochastic optimization. *arXiv preprint arXiv:1412.6980*, 2014.
- Koyama, M. and Yamaguchi, S. When is invariance useful in an out-of-distribution generalization problem? *arXiv preprint arXiv:2008.01883*, 2020.
- Kusner, M. J., Loftus, J., Russell, C., and Silva, R. Counterfactual fairness. *Advances in neural information processing systems*, 30, 2017.
- Li, Y., Wang, Y., and Cui, Z. Decoupled multimodal distilling for emotion recognition. In *Proceedings of the IEEE/CVF Conference on Computer Vision and Pattern Recognition*, pp. 6631–6640, 2023.
- Liang, V. W., Zhang, Y., Kwon, Y., Yeung, S., and Zou, J. Y. Mind the gap: Understanding the modality gap in multi-modal contrastive representation learning. *Advances in Neural Information Processing Systems*, 35: 17612–17625, 2022.
- Lu, J., Clark, C., Zellers, R., Mottaghi, R., and Kembhavi, A. Unified-io: A unified model for vision, language, and multi-modal tasks. In *The Eleventh International Conference on Learning Representations*, 2022.
- Ma, H., Han, Z., Zhang, C., Fu, H., Zhou, J. T., and Hu, Q. Trustworthy multimodal regression with mixture of normal-inverse gamma distributions. *Advances in Neural Information Processing Systems*, 34:6881–6893, 2021.
- Mahesh, B. Machine learning algorithms-a review. *International Journal of Science and Research (IJSR)*. [Internet], 9(1):381–386, 2020.
- Menze, B. H., Jakab, A., Bauer, S., Kalpathy-Cramer, J., Farahani, K., Kirby, J., Burren, Y., Porz, N., Slotboom, J., Wiest, R., et al. The multimodal brain tumor image segmentation benchmark (brats). *IEEE transactions on medical imaging*, 34(10):1993–2024, 2014.
- Morgan, S. L. and Winship, C. *Counterfactuals and causal inference*. Cambridge University Press, 2015.
- Niu, T., Zhu, S., Pang, L., and El Saddik, A. Sentiment analysis on multi-view social data. In *MultiMedia Modeling: 22nd International Conference, MMM 2016, Miami, FL, USA, January 4-6, 2016, Proceedings, Part II 22*, pp. 15–27. Springer, 2016.
- Pearl, J. *Causality*. Cambridge university press, 2009.
- Radford, A., Kim, J. W., Hallacy, C., Ramesh, A., Goh, G., Agarwal, S., Sastry, G., Askell, A., Mishkin, P., Clark, J., et al. Learning transferable visual models from natural language supervision. In *International conference on machine learning*, pp. 8748–8763. PMLR, 2021.
- Silberman, N., Hoiem, D., Kohli, P., and Fergus, R. Indoor segmentation and support inference from rgbd images. In *Computer Vision—ECCV 2012: 12th European Conference on Computer Vision, Florence, Italy, October 7-13, 2012, Proceedings, Part V 12*, pp. 746–760. Springer, 2012.
- Song, S., Lichtenberg, S. P., and Xiao, J. Sun rgb-d: A rgb-d scene understanding benchmark suite. In *Proceedings of the IEEE conference on computer vision and pattern recognition*, pp. 567–576, 2015.
- Sun, Q., Fang, Y., Wu, L., Wang, X., and Cao, Y. Evalclip: Improved training techniques for clip at scale. *arXiv preprint arXiv:2303.15389*, 2023.
- Suter, R., Miladinovic, D., Schölkopf, B., and Bauer, S. Robustly disentangled causal mechanisms: Validating deep representations for interventional robustness. In *International Conference on Machine Learning*, pp. 6056–6065. PMLR, 2019.

- Tian, J. and Pearl, J. A general identification condition for causal effects. In *Aaai/iaai*, pp. 567–573, 2002.
- Wang, H., Chen, Y., Ma, C., Avery, J., Hull, L., and Carneiro, G. Multi-modal learning with missing modality via shared-specific feature modelling. In *Proceedings of the IEEE/CVF Conference on Computer Vision and Pattern Recognition*, pp. 15878–15887, 2023a.
- Wang, H., Ma, C., Zhang, J., Zhang, Y., Avery, J., Hull, L., and Carneiro, G. Learnable cross-modal knowledge distillation for multi-modal learning with missing modality. In *International Conference on Medical Image Computing and Computer-Assisted Intervention*, pp. 216–226. Springer, 2023b.
- Wang, J., Wang, Z., Tao, D., See, S., and Wang, G. Learning common and specific features for rgb-d semantic segmentation with deconvolutional networks. In *Computer Vision–ECCV 2016: 14th European Conference, Amsterdam, The Netherlands, October 11–14, 2016, Proceedings, Part V 14*, pp. 664–679. Springer, 2016.
- Wang, J., Mou, L., Ma, L., Huang, T., and Gao, W. Amsa: adaptive multimodal learning for sentiment analysis. *ACM Transactions on Multimedia Computing, Communications and Applications*, 19(3s):1–21, 2023c.
- Wang, J., Qiang, W., Ren, Y., Song, Z., Zhang, J., and Zheng, C. Hacking task confounder in meta-learning. *arXiv preprint arXiv:2312.05771*, 2023d.
- Wang, P., Yang, A., Men, R., Lin, J., Bai, S., Li, Z., Ma, J., Zhou, C., Zhou, J., and Yang, H. Ofa: Unifying architectures, tasks, and modalities through a simple sequence-to-sequence learning framework. In *International Conference on Machine Learning*, pp. 23318–23340. PMLR, 2022.
- Wang, X., Kumar, D., Thome, N., Cord, M., and Precioso, F. Recipe recognition with large multimodal food dataset. In *2015 IEEE International Conference on Multimedia & Expo Workshops (ICMEW)*, pp. 1–6. IEEE, 2015.
- Wu, F., Jing, X.-Y., Wu, Z., Ji, Y., Dong, X., Luo, X., Huang, Q., and Wang, R. Modality-specific and shared generative adversarial network for cross-modal retrieval. *Pattern Recognition*, 104:107335, 2020.
- Xia, Y., Huang, H., Zhu, J., and Zhao, Z. Achieving cross modal generalization with multimodal unified representation. *Advances in Neural Information Processing Systems*, 36, 2024.
- Xu, P., Zhu, X., and Clifton, D. A. Multimodal learning with transformers: A survey. *IEEE Transactions on Pattern Analysis and Machine Intelligence*, 2023.
- Yang, D., Kuang, H., Huang, S., and Zhang, L. Learning modality-specific and-agnostic representations for asynchronous multimodal language sequences. In *Proceedings of the 30th ACM International Conference on Multimedia*, pp. 1708–1717, 2022.
- Yang, M., Zhang, Y., Fang, Z., Du, Y., Liu, F., Ton, J.-F., Wang, J., and Wang, J. Invariant learning via probability of sufficient and necessary causes. *Advances in Neural Information Processing Systems*, 36, 2024.
- Zhang, Q., Wang, Y., and Wang, Y. On the generalization of multi-modal contrastive learning. In *International Conference on Machine Learning*, pp. 41677–41693. PMLR, 2023a.
- Zhang, Q., Wu, H., Zhang, C., Hu, Q., Fu, H., Zhou, J. T., and Peng, X. Provable dynamic fusion for low-quality multimodal data. In *International conference on machine learning*, pp. 41753–41769. PMLR, 2023b.
- Zhang, Q., Wu, H., Zhang, C., Hu, Q., Fu, H., Zhou, J. T., and Peng, X. Provable dynamic fusion for low-quality multimodal data. In *International conference on machine learning*, pp. 41753–41769. PMLR, 2023c.
- Zhang, Q., Wu, H., Zhang, C., Hu, Q., Fu, H., Zhou, J. T., and Peng, X. Provable dynamic fusion for low-quality multimodal data. In *International conference on machine learning*, pp. 41753–41769. PMLR, 2023d.
- Zhang, Y., Yang, J., Tian, J., Shi, Z., Zhong, C., Zhang, Y., and He, Z. Modality-aware mutual learning for multimodal medical image segmentation. In *Medical Image Computing and Computer Assisted Intervention–MICCAI 2021: 24th International Conference, Strasbourg, France, September 27–October 1, 2021, Proceedings, Part I 24*, pp. 589–599. Springer, 2021.
- Zhang, Y., He, N., Yang, J., Li, Y., Wei, D., Huang, Y., Zhang, Y., He, Z., and Zheng, Y. mmformer: Multimodal medical transformer for incomplete multimodal learning of brain tumor segmentation. In *International Conference on Medical Image Computing and Computer-Assisted Intervention*, pp. 107–117. Springer, 2022.
- Zhou, T., Fu, H., Chen, G., Zhou, Y., Fan, D.-P., and Shao, L. Specificity-preserving rgb-d saliency detection. In *Proceedings of the IEEE/CVF international conference on computer vision*, pp. 4681–4691, 2021.